Surfaces and Interfaces 36 (2023) 102524

Contents lists available at ScienceDirect

Surfaces and Interfaces

journal homepage: www.sciencedirect.com/journal/surfaces-and-interfaces

Influence of roughness and coating on the rebound of droplets on fabrics

Patrick James Cruz, Pierre-Paul De Breuck, Gian-Marco Rignanese, Karine Glinel, Alain M. Jonas *

Institute of Condensed Matter and Nanosciences, Université Catholique de Louvain, Croix du Sud 1, Louvain-la-Neuve 1348, Belgium

ARTICLE INFO

Keywords:
Textiles
Impacting droplets
Water roll-off
Wetting

ABSTRACT

We investigate the behavior of small water droplets impacting fabrics of different roughness and coating type in a range of impacting conditions, and compare it to measurements of static and roll-off angles. Fabrics with low roughness display lower static contact angle, no roll-off, a slightly slower retraction rate for impacting droplets, a narrower Weber number (*We*) range in which rebound occurs, and a limited maximum rebound at intermediate *We*. Rougher fabrics exhibit slightly higher static contact angles, lower roll-off angles, a slightly faster retraction rate for impacting droplets, and a larger *We* range for rebound; additionally, the restitution of kinetic energy upon rebound is proportional to 1/*We*, indicating a near-to-constant rebound height independent of the impact velocity. As regards coating type, roll-off angle, *We* range for rebound, and to a lesser extent restitution coefficient, depend on coating type, with the more environmentally-friendly wax-based coating being superior to silicone and perfluorobutyl-based ones in both drop impact and roll-off experiments. Our results thus provide hope that perfluorinated coatings can be eliminated in standard textiles, and provide an extensive view of how roughness, coating and impact conditions control the fate of small droplets falling on textiles.

1. Introduction

Water repellency is a critical property of daily-life fabrics, to protect us outdoors during rainy seasons. Traditionally, coatings providing water repellency to fabrics have largely been based on perfluoroalkylated oligomers, owing to their exceptional water and oil repellency [1]. However, perfluorinated alkyl derivatives rise severe environmental concerns associated to their accumulation in the environment [2], as well as to their industrial synthesis (as exemplified in popular culture by the Dark Waters movie directed by Todd Haynes in 2019, or by the recent discovery of a large-scale perfluorooctanesulfonic acid pollution at Zwijndrecht, Belgium, potentially affecting the life of tens of thousands).

Consequently, a regulatory ban of perfluorooctyl derivatives is being implemented for textiles in the EU and other countries [3]. Alternative water-repellent coatings are therefore proposed in the fabrics industry, ranging from hardly safer [4] shorter perfluoroalkyls (*e.g.*, perfluorobutyl) to probably much more innocuous wax-based materials, and including silicone-based formulations (which are however also environmentally-criticized owing to the toxicity of cyclic silicones [5]) and waterborne polyurethanes [6].

In this context, it is important to critically analyze the performance of these new alternative formulations with respect to their wetting performance, which will allow us to balance their properties against possible environmental threats they may pose. When performing such an analysis, it is crucial to include the effect of the fabric texture on the wetting properties. Indeed, fabrics display an inherent roughness due to the weaving of threads. This may favorably contribute to increasing their overall water-repellency since surface roughness is an important contributor to wetting properties through the entrapment of air pockets at the fabric surface.

Some of us have previously reported on the static water contact θ and roll-off angles θ_{RO} of a range of fabrics coated by different hydrophobic formulations [7]. This previous study revealed that fabrics of higher roughness are associated to larger water contact angles with little dependence on the nature of the coating. A higher roughness is also generally conducive to a lower roll-off angle (the tilt angle away from horizontality from which a droplet starts to roll off a surface), with a strong dependence on coating type. Coatings having lower values of pinning parameter μ were found to be generally superior in this respect, with $\mu = \gamma(\cos\theta_{rec} - \cos\theta_{adv})$ in which γ is the water surface tension, and θ_{adv} and θ_{rec} are the advancing and receding water contact angles measured on a flat surface, respectively. The pinning parameter represents the wetting hysteresis on a flat surface, which results partly from dissipative

* Corresponding author.
E-mail address: Alain.jonas@uclouvain.be (A.M. Jonas).

https://doi.org/10.1016/j.surfin.2022.102524
Received 3 November 2021; Received in revised form 6 November 2022; Accepted 24 November 2022
Available online 25 November 2022

mechanisms acting during the spreading of a droplet. The roll-off angle is thus a measure of wetting dynamics and is consequently an important parameter for protective clothes. However, it does not capture the dynamic behavior of droplets *falling* on such fabrics.

There is growing research on the water repellency of fabrics, focusing on new coatings or roughness design by weaving [7–12]. However, most of these studies simply evaluate static wettability, even though dynamic wettability is more relevant for typical applications, *e.g.*, when raining. Dynamic wettability is commonly evaluated by studying the impact dynamics of droplets on fabrics, including the computation of the restitution coefficient R_C based on the rebound velocity of the impacting droplet. This coefficient R_C is related to the amount of energy recovered by the droplet after impact, and is expressed as $R_C = V_{AR} / V_0$, where V_{AR} and V_0 are the after-rebound and initial impact speeds, respectively. On high-quality superhydrophobic surfaces, droplets rebound close to their dropping heights, leading to values of R_C close to 1 [13]. Another useful parameter in droplet impact dynamics is the Weber number *We*, which provides the balance between the initial kinetic energy and the surface energy of the droplet, and therefore depends on the dropping height (through V_0) and droplet size: $We = \rho V_0^2 D_o / \sigma$, where ρ and σ are density and surface tension of the fluid, respectively, and D_o is the initial droplet diameter.

Unfortunately, whereas there are droplet impact studies specific to textiles or fabric-based composites [10,14–16], they do not focus on understanding water repellency based on droplet rebound. Here, we demonstrate that woven fabrics having different weave microstructures and different coating formulations create a wide range of dynamic water repellency behavior — from which we identify the relevant parameters affecting such behavior. Their static water repellency is characterized by measuring the contact angle of droplets on these fabrics; their dynamic water repellency is characterized by the roll-off angle and impact behavior of water droplets. Seven fabrics are considered, six of them being plain-woven, while the remaining one is twill-woven with two different sides — giving eight unique fabric surfaces overall. Three water-based formulations are used as hydrophobic coating for these fabrics: a perfluorobutyl-modified polyurethane emulsion, a silicone-based emulsion and a wax-modified resin dispersion.

Our work thus concentrates on the influence of fabric roughness and coating type on the dynamic water repellency of woven fabrics by investigating their interaction with water droplets for different values of *We*. We demonstrate that the selection of an appropriate fabric microstructure can considerably improve the water repellency of fabrics, and that the environmentally-more friendly wax-based coatings appear to be superior to short perfluoroalkyl chains and silicone-derived coatings.

2. Experimental section

2.1. Materials and preparation of coated fabrics

The samples used are polyester fabrics provided by textile manufacturers, based on fibers of similar diameter (10-25 μm). The roughness *r* of each fabric was determined experimentally in a previous work [7] and is collected in Table 1; roughness is here defined as the ratio of the actual (probed) area to the projected area of the fabric surface, as measured by stylus profilometry ($r \geq 1$).

The characteristics of the hydrophobic formulations used as coatings are provided in Table 2. Dip-coating was performed to prepare the coated fabric samples. The commercial *PhobRSH* formulation was diluted with acidified water (pH 4.0 – 5.0) by a factor of 25, using Milli-Q water (resistivity 18.2 MΩ.cm, obtained from a Merck Millipore system). A crosslinker formulation, *Phobol Extender XAN*, was then added to the acidified diluted *PhobRSH* suspension in a ratio of 1:250 by mass. The *C4F* and *PDMS* suspensions were simply diluted until a final concentration of 1.5 wt. % solid. Next, the fabric samples were dip-coated in these diluted coating suspensions for 3 min. After being suspended in air for a few seconds, they were placed on a hot plate at 150°C for some time (5 min for *PhobRSH*, and 3 min for *C4F* and *PDMS* formulations) to dry and crosslink the polymer of the coating. Finally, after cooling, the coated fabrics were fixed on glass substrates with adhesive tape to minimize their deformation during droplet impact studies. The typical thickness of the films obtained by dip-coating was found to be *ca.* 250 nm (Supplementary Information, Fig. S1).

Table 1
Characteristics of the polyester fabrics of this study.

Fabric number	Weave Type	*r*	Fiber diameter, in warp/wept directions (μm)	Unit cell dimensions (μm × μm)	Defect density[a]
1	plain	1.19	10/20	600 × 400	Low
2	plain	1.27	15/25	600 × 750	Low
3	plain	1.46	22/20	340 × 550	Low
4	plain	1.47	18/22	310 × 680	High
5	plain	1.77	16/18	730 × 810	Medium
6	plain	1.77	20/16	540 × 350	High
7A	twill	1.71	12/14	330 × 450	Medium
7B	twill	1.67	16/12	540 × 550	Medium

[a] Number of defects per surface area: Low: less than 1.4/mm^2; High: more than 2.8/mm^2. Defects are typically loose threads and loops or dangling fiber ends.

Additionally, flat samples were prepared by spin-coating on silicon wafers at 3000 rpm for 30 s, then annealing at 150°C for 2 min. These flat samples were coated with an undiluted *PDMS* suspension, with a *C4F* suspension diluted by a factor 2, or with a 10:1 mixture of undiluted *PhobRSH* and *Phobol Extender XAN*.

2.2. Contact and roll-off angle measurements

These were performed with an OCA 20 goniometer from Dataphysics. Contact angle (θ) measurements were performed at six different positions by gently depositing a 10.0 μL water droplet on fabric surfaces in sessile drop fashion. The drawing of the droplet-fabric interface baseline was often difficult, particularly for samples with inherently rough surfaces — resulting in some uncertainty. Roll-off angle (θ_{RO}) measurements were performed at four different positions: a 10.0 μL water droplet was initially deposited on the fabric, and subsequently allowed to roll off by progressively tilting the sample stage. Finally, the measurement of advancing and receding contact angles was performed with an initial 5.0 μL water droplet using the flat samples as described in previous work [7].

2.3. Droplet impact studies and extraction of relevant parameters

The droplet behavior on different fabrics was surveyed by recording videos using a high-speed camera at a frequency of ~900 frame per second and an optical resolution of ~16.7 μm-per-pixel. The water droplets were dispensed from the 500 μL electronically-controlled Hamilton syringe pump of the OCA 20 goniometer. Two values of droplet diameter (*ca.* 1.9 and 2.7 mm) and a range of dropping heights (from *ca.* 5 to 200 mm) were considered. This gives a wide range of droplet dynamic behavior with different impact speeds and droplet diameters, from which an experimental *We* range ($1 < We < 120$) was obtained, which comprises the lower range of *We* for natural rainfalls [17]. Each observation (video) thus corresponds to a water droplet of certain volume impacting a specific coated fabric from a given dropping height. It was assumed that prior to impact, the droplet has kept its volume and its spherical shape, allowing to neglect the influence of evaporation and shape asymmetry, respectively. The amount of information captured in some videos was limited due to the tradeoff between spatial/temporal resolution and field of view of camera; this includes cases where either the maximum height of the main droplet or of the tiny secondary droplets ejected from it during rebound was exceptionally high.

Table 2
Description of hydrophobic coatings.

Commercial Name	Composition	Abbreviated Name	θ [a] (°)	θ_{adv} [b] (°)	θ_{rec} [c] (°)	Pinning parameter μ (N/m)
Phobotex RSH	Water-based wax-modified resin	*PhobRSH*	105	113	95	0.022
3M™ PM 900	Water-based emulsion of fluoropolymer (perfluorobutyl-modified polyurethane)	*C4F*	110	116	42	0.086
Wacker HC303	Water-based silicone emulsion	*PDMS*	111	108	85	0.029

[a] Static contact angle
[b] Advancing contact angle
[c] Receding contact angle. The angles were measured on silicon wafers spin-coated with the coating formulations.

The videos were analyzed using in-house routines developed in *Wavemetrics Igor Pro* and *Python*. The rebound behavior of droplets was quantified solely from its translational motion along the vertical direction, *i.e.*, the movement of its center of mass normal to the fabric surface. The vibrations of droplets observed in a few videos were thus not accounted for in this work, and an in-house height threshold was set to distinguish rebounding droplets from non-rebounding and oscillating droplets close to resting. The following parameters were extracted from each video: (a) rebound height, H_B; (b) contact width upon maximal extension of the droplet on the fabric surface, $D_{contact}$; (c) equilibrium contact width, D_{eq}; (d) maximum receding rate after maximal extension on the fabric, $V_{R,max}$; (e) time-average number of droplets, N_d; and (f) impact speed V_0. The after-impact droplet speed V_{AI}, in contrast, was simply approximated using the free-fall formula: $V_{AI} = (2gH_B)^{1/2}$, where g is the acceleration due to gravity. From these values, the parameters *We* and R_C were computed. However, the difficulty in determining droplet-fabric interface also affected the determination of $D_{contact}$.

2.4. Principal component analysis

(PCA) was used to describe the influence of different fabric parameters on the global impact behavior of droplets. After removing the parameters related to droplet characteristics, the remaining following five features from the extracted video parameters were considered: (a) $\xi_{max} = D_{contact} / D_o$ with D_o the initial droplet diameter, (b) R_C, (c) equilibrium contact width D_{eq}, (d) maximum receding rate $V_{R,max}$, and (e) time-average number of droplets N_d. All sets of parameters were standardized to zero average and unit standard deviation, to remove the influence of the actual magnitude of each parameter. The first two principal components were then plotted to create the final visual representation of droplet dynamics.

3. Results and discussion

3.1. Static contact angle and roll-off angle on coated fabrics

The tested fabrics demonstrated a wide range of roughness r and surface quality, owing mostly to the specific packing of fibers of different diameters in the yarns, as fully described in Ref. [7] and summarized in Table 1; profilometry images of the fabrics are displayed in Supplementary Fig. S2. Here, the roughness is defined as the ratio between the developed area of the external fabric surface to its projected area; a roughness of 1 thus corresponds to a perfectly flat surface, whereas a roughness of 1.5 corresponds to 50% added surface due to the corrugations of the fabric. Full information on the roughness of fabrics is in Ref. [7].

Different coating formulations were then deposited on the fabrics as described in the experimental section. After coating, the wetting behavior of the fabrics changed dramatically: whereas water droplets rapidly impregnated uncoated fabrics, they displayed contact angles larger than 120° on coated fabrics, testifying for the proper chemical modification of the fabric surface by a coating layer thicker than at least a few nanometers [18]. This is in agreement with our experimental estimations of coating thickness, which indicate thicknesses in the range of 250 nm (Supplementary Fig. S1). Of note, profilometry measurements performed before and after coating did not detect a significant change of roughness [7], testifying for the smoothness of the coatings at the sub-micrometer scale. Fig. 1 shows how the contact angle θ increases with fabric roughness, passing successively by two regimes as fully discussed before [7]. At low roughness, the fabric surfaces are in a partially-impregnated state, in which the droplet penetrates within the top layer of the fabric and fills its superficial cavities. At higher roughness, the fabrics are in a superficially-wet state, for which the droplet rests over trapped air pockets and only touches the topmost surface of the external fibers. These regimes are essentially similar to the Wenzel [19] and Cassie and Baxter [20] states, respectively, as commonly found for rough surfaces, including superhydrophobic surfaces [21,22].

Water droplets only roll or slide on the fabrics in the superficially-wet regime; since a higher roughness increases the amount of trapped air pockets, it also generally results in lower roll-off angles θ_{RO} (Fig. 1). Additionally, coatings of lower pinning parameter μ (such as the wax-based *PhobRSH*) tend to display lower roll-off angles for a given roughness, since the work needed for sliding or rolling decreases for lower μ [7,23–25]. However, these relationships are not univocal because roll-off is also influenced by other parameters describing the topography and quality of the fabric surface. Defects such as fiber loops and protrusions, for example, can pin the water droplet in certain samples. These general observations are in good agreement with the physical model developed in Ref. [7], which can be fitted satisfactorily to the new experimental data (dashed lines, Fig. 1).

3.2. Droplet impact dynamics on coated fabrics

Droplets impacting on fabrics exhibit a range of behavior, depending on *We* and fabric texture. A graphical survey of different possible scenarios is displayed in Fig. 2; all 2010 videos are freely accessible at https://dataverse.uclouvain.be/dataverse/DropletVideos.

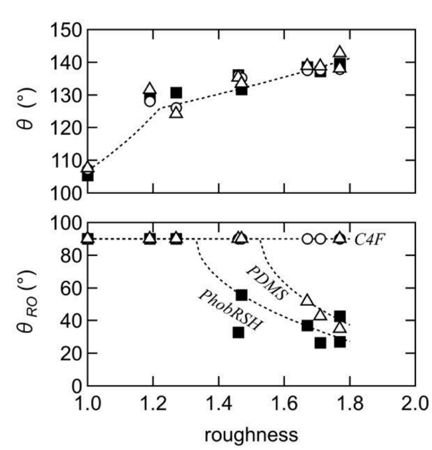

Fig. 1. Static contact angle θ and roll-off angle θ_{RO} versus fabric roughness r for the three coating types (squares: *PhobRSH*; triangles: *PDMS*; circles: *C4F*). Roll-off angles of 90° are used to indicate the absence of roll-off. The dashed lines are fits of a theoretical model [7] to the data.

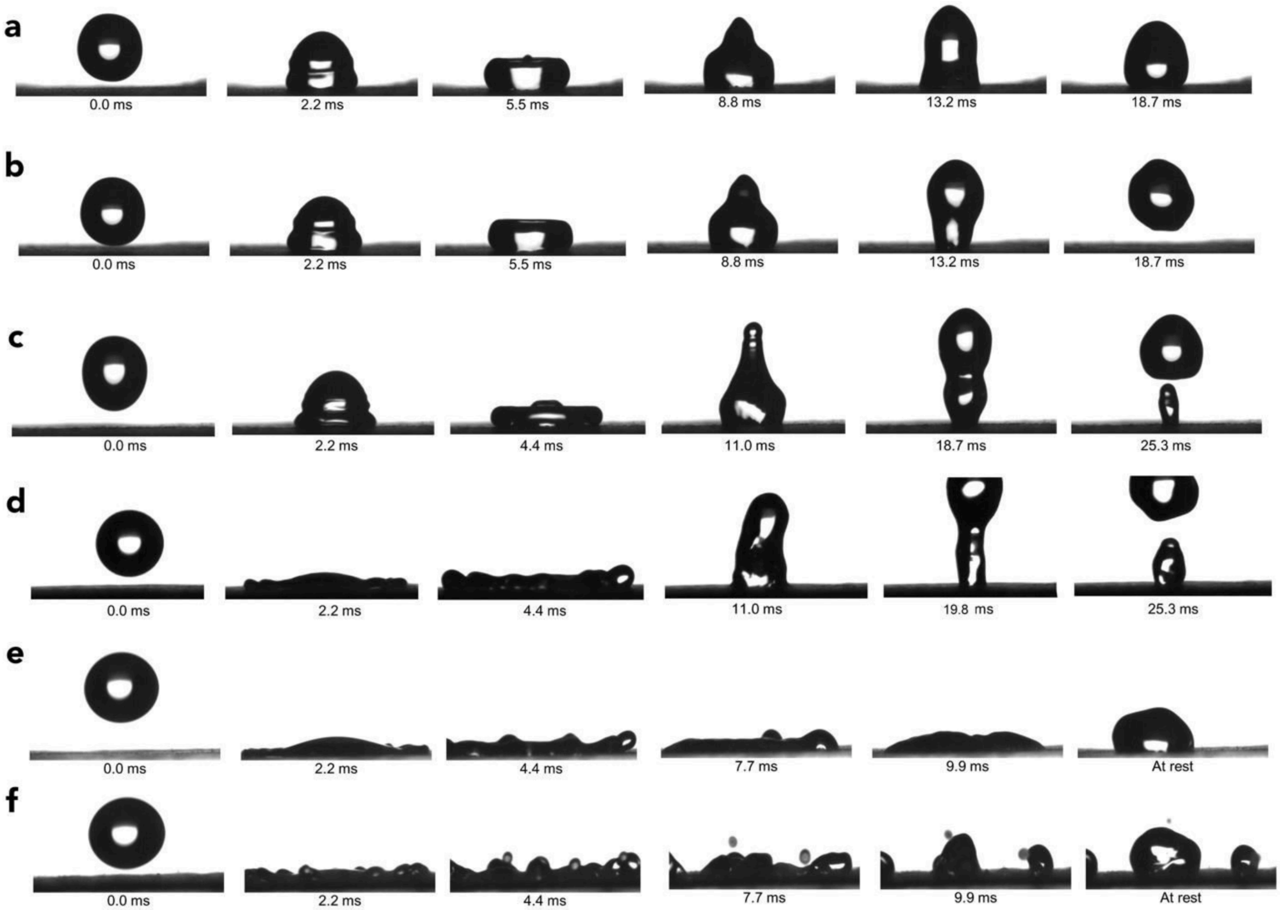

Fig. 2. Typical behavior of droplets of 2.7 mm diameter impacting fabric samples, with *We* number/impact speed in m/s increasing from top to bottom: (a-b) 3.6/0.3; (c) 17.1/0.7; (d) 69.9/1.4; (e-f) 90.8/1.6. Samples are *PhobRSH*-coated fabrics of different roughness: (a) Fabric 2, r=1.27; (b–d) Fabric 7A, r=1.71; (e) Fabric 1, r=1.19; (f) Fabric 5, r=1.77.

The droplets first spread laterally shortly after impact (4-5 ms); for higher values of *We* and rougher fabrics, they may fragment in smaller droplets upon spreading (*i.e.*, splashing, Fig. 2f). The frequency of occurrence of splashing is reported in Fig. S3; high *We* numbers, a large roughness and/or an increased amount of fabric defects (Table 1) generally favor splashing. The droplet then retracts and may either stick on the surface, typically for low *We* and fabric roughness (Fig. 2a), rebound (Fig. 2b) or partially rebound with or without jetting (Fig. 2c, d) for intermediate *We*, or be impaled and stick on the fabric (pinning, Fig. 2e, f) typically for higher *We* numbers. In the sequel, we will essentially focus on the spreading and rebound behavior of droplets on the fabrics, for which a consistent set of conclusions could be reached with our experiments.

3.2.1. *Spreading behavior of impacting water droplets*

After impact, the droplet flattens and spreads outward radially until it reaches its maximum spreading diameter $D_{contact}$. Fig. 3 shows the variation of $\xi_{max} = D_{contact} / D_o$ with D_o the initial droplet diameter, across samples of different fabric roughness, coating type and impact conditions.

All values collapse over a broad master curve, consistent with previous work on both smooth [26] and rough [27] solid surfaces, as well as on textiles made of densely-packed fibers [14]. The maximum contact width of the droplet is thus essentially independent of the roughness of the fabric over which it spreads, and the chemical nature of the hydrophobic coating does not significantly influence ξ_{max} either. Clanet et al. [26] proposed that when $We >> 1$, the shape of the maximally-spread droplet is fully governed by the considerably increased gravity field resulting from the deceleration, which completely overcomes surface forces and therefore the details of the water/fabrics interface. In this regime, ξ_{max} was predicted to scale as

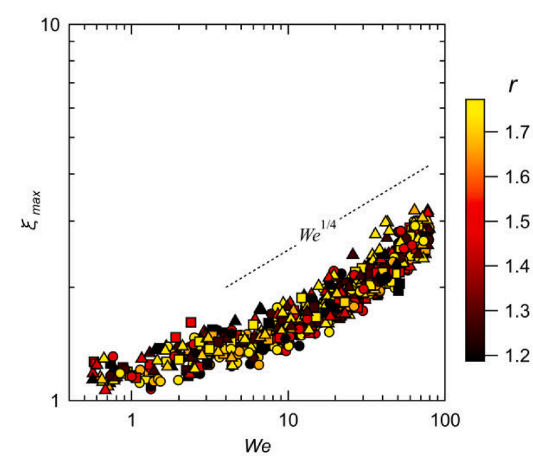

Fig. 3. Master curve (logarithmic axes) of the dimensionless maximum contact width ξ_{max} versus Weber number *We* for all samples and probed experimental conditions (including two different droplet diameters and a large range of dropping heights). Each point corresponds to one video observation. The color code refers to the roughness r of the fabrics; symbols refer to the coating nature (squares: *PhobRSH*; triangles: *PDMS*; circles: *C4F*). The dashed line is the scaling law predicted by the model of Clanet et al. [26] when $We >> 1$.

$We^{1/4}$, which is indeed reasonably well followed by our experimental data (Fig. 3), although the limited range of ξ_{max} values limits the confidence on the exact value of this experimental scaling exponent [28]. At lower We, the impacting droplet does not form a puddle anymore and its maximal width then deviates from the $We^{1/4}$ scaling law. At any rate, ξ_{max} is clearly not following the scaling law $\xi_{max} \sim (We+1)^{1/2}$ which is expected when all the kinetic energy of the droplet is transformed into surface energy upon spreading in a thin puddle [29]. This demonstrates that a significant portion of the kinetic energy is dissipated during spreading, with the dissipated fraction increasing with We.

3.2.2. Rebound behavior of impacting water droplets

The droplet may or may not rebound after retraction: the exact outcome will depend on the amount of stored surface/interfacial energy at maximum spreading, among other several factors. Fig. 4 shows the restitution coefficient R_C over the probed We range, for all samples and coating types.

No droplet rebound is observed before a critical value of We, due to the dissipation of part of the kinetic energy upon impact. The two fabrics of lower roughness (Fabrics 1 and 2), for which static droplets gently deposited on the surface settle in the partially-impregnated regime or close to it (Fig. 1), have an especially high threshold for rebound. This is most probably due to the pinning of the droplet on the fabrics, resulting from partial impregnation which increases the energy needed for detachment. This hypothesis is supported by the measurement of the maximal rate of retraction of the droplet/fabric interface after maximal spreading (Fig. 5). On fabrics of roughness below *ca.* 1.3 (black and dark-brown points in Fig. 5), which are in or close to the partially-impregnated regime, the droplets display a significantly lower retraction rate compared to rougher fabrics, which testifies for a higher interfacial friction. This contrasts with the maximal spreading (Fig. 3), which was found to be independent of roughness. Of note, as for the maximal spreading, no significant difference between the different coating types was observed in the maximal retraction rate.

We observed that, above the minimal threshold, rebound may or not occur depending on We and roughness, and fully disappears above a second threshold value due to (partial) impalement of the droplet and subsequent pinning upon retraction. Fig. 6 provides a pictorial representation of these results in a (r, We) map, with gray regions indicating conditions for which droplets dominantly rebound. Very generally, droplets rebound for a limited range of We values, which widens when

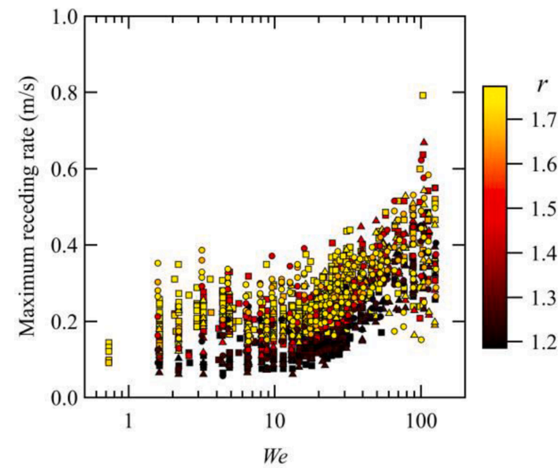

Fig. 5. Maximal value of the retraction rate of the droplet/fabric interface after maximal spreading, for fabrics of different roughness (color code) and different coatings (squares: *PhobRSH*; triangles: *PDMS*; circles: *C4F*).

the roughness increases; however, a detailed examination of Fig. 4 reveals that some fabrics may deviate from these general considerations. This is especially the case of Fabric 4, over which rebound is less favored than expected, probably due to its quite high concentration of surface defects (Table 1).

The range within which rebound can occur is thus driven by interfacial tension with the fabric surface. Therefore, droplet rebound can be sensitive to the exact characteristics of the local surface: the intrinsic variability present in each fabric creates a range of rebound behavior for droplets at close or even equal magnitude of We, which is why fabrics having a larger amount of surface defects (such as Fabric 4) may deviate from the general trends. Interestingly, in the rebound regime (gray zones in Fig. 6), the $R_C(We)$ data obtained for different fabrics with one specific coating superimpose to form master curves displaying a $R_C \sim We^{-1/2}$ scaling relationship (Fig. 7). Of note, Fabric 4 was excluded when plotting these data, due to its high number of surface defects which results in deviations from this relationship.

The scaling law corresponds well to the prediction of the model of Biance et al. [30], which applies for large We and droplets smaller than the capillary length of water. In this model, the vertical speed at droplet

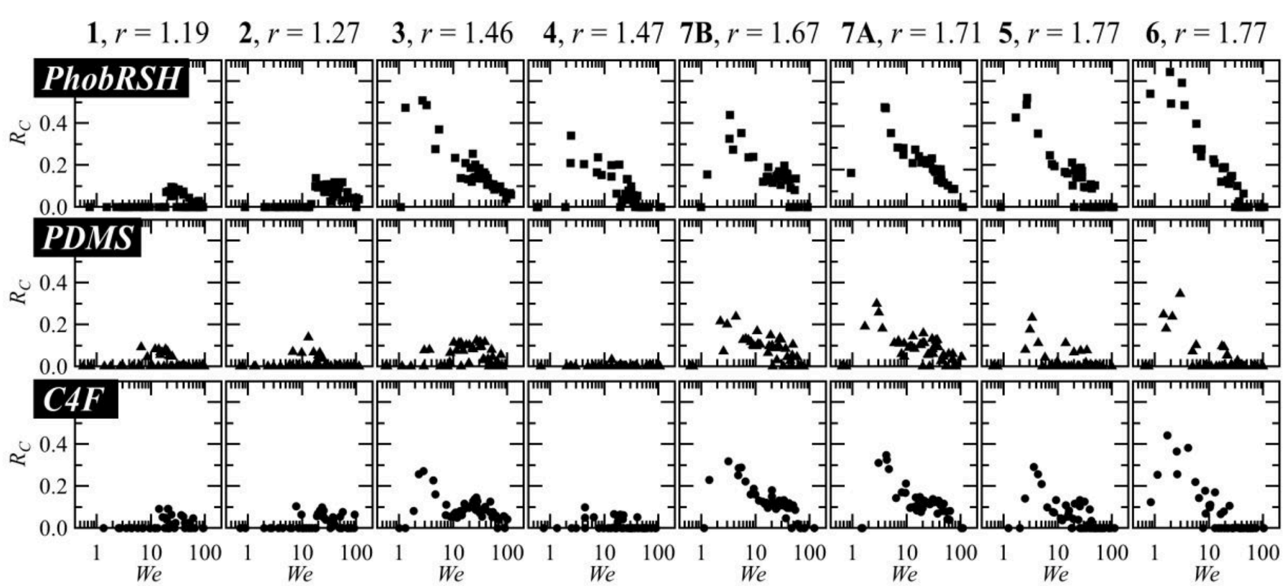

Fig. 4. Restitution coefficient R_C versus Weber number We, for the different fabrics (columns, with fabric number and roughness r indicated at the top), for three different coatings (rows). Each point corresponds to one video observation.

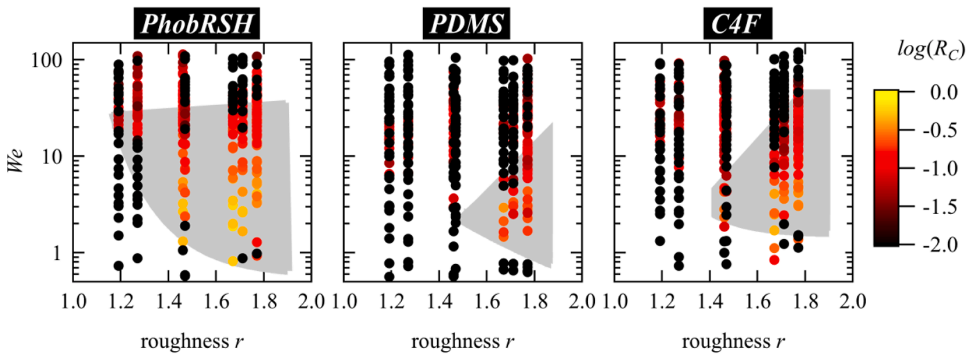

Fig. 6. Map of the restitution coefficient R_C of water droplets impinging on the fabrics, depending on *We* and fabric roughness. The color code indicates the value of R_C, with black dots corresponding to the absence of droplet rebound ($R_C < 0.01$). The grayed zone corresponds to the region in which rebound often occurs.

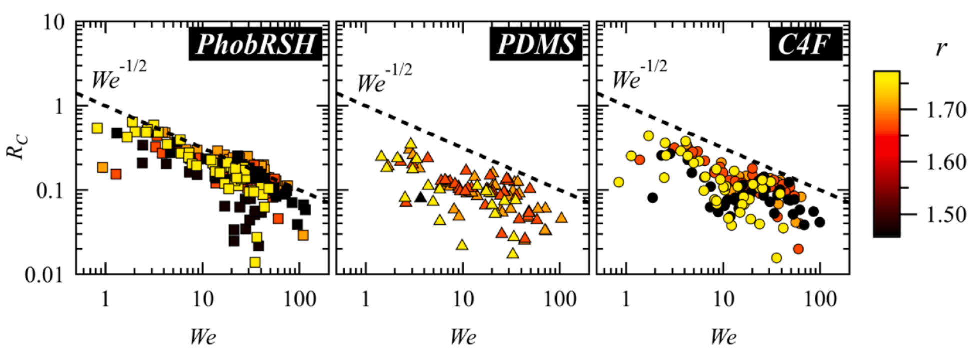

Fig. 7. Restitution coefficient versus Weber number for all fabrics in the gray rebound zones of Fig. 6 (except Fabric 4), depending on coating type. The dashed lines show $R_C = We^{-1/2}$. The color code indicates the roughness of the fabrics.

take-off is independent of the impact speed and is defined by the natural oscillation frequency of the droplet which only depends on its mass, radius, and surface tension. Accordingly, when rebounding, the droplets always reach an identical maximal height on the order of $\gamma/g\rho D_0$ [30]. For droplets of 2-3 mm diameter as used here, this corresponds to a height of *ca.* 3 mm, which is indeed observed in our experiments (Fig. S4).

However, the model does not consider the adhesion force between the droplet and surface, which does not change the scaling exponent but slightly modulates the absolute value of the restitution coefficient. As Fig. 7 shows, the scaling law which applies to *PDMS*-coated fabrics lies on average slightly lower than the one of *C4F*-coated fabrics, which is itself slightly lower than for wax-coated fabrics. This is similar as the size of the rebounding regime regions in the maps of Fig. 5, which is smaller for *PDMS* compared to *C4F*, itself smaller compared to what is found for *PhobRSH*-based coatings.

Altogether, Figs. 6 and 7 thus show that droplet adhesion and energy dissipation increase from wax- to *C4F*- to *PDMS*-based coatings. Among the three coatings, *PhobRSH* is also the one with the lowest pinning parameter μ (or, equivalently, contact angle hysteresis $\Delta\theta$)— which is the origin for the lower θ_{RO} for its corresponding fabrics. Unlike spreading, the rebound of droplets thus appears to be affected by the surface friction resulting from the coating, which is in part tied to its corresponding μ. Stated otherwise, the influence of the coating is the result of the higher θ_{rec} of *PhobRSH* but similar θ_{adv} compared to the other two coatings, as proposed in another work on solid surfaces [31].

The $R_C \sim We^{-1/2}$ scaling law also indicates that, for high impact velocities, the advantage of a specific coating or of a rougher fabric surface will necessarily be lost. Additionally, droplet pinning due to impalement (and splashing) starts to occur when a sufficiently high *We* is reached. This impalement is accompanied by the dissipation of available energy and ultimately the suppression of rebound, marking the eventual wetting of fabric surfaces. Finally, the model of Biance et al. [30]. applies to small droplets of a size below the capillary length of water, as used here. Droplets above that size (*ca.* 2.7 mm at room temperature) are dominated by gravity, not surface tension. As a result, they generally do not rebound whatever the impact velocity, as was demonstrated experimentally in another context [30].

3.3. Correlation between impact behavior and roll-off of water droplets

It has been shown earlier that, even for fabrics in the superficially wet regime with a high fraction of air pockets, impacting droplets do not necessarily display a high rebound. Therefore, while the contact angle θ of a static droplet can be used to classify the fabrics based on impregnation regimes, it does not predict the water repellency in a drop impact test. Such a prediction could be made easier by using the roll-off angle θ_{RO}, which is sensitive to the pinning parameter and hysteresis phenomena that also influence the impact behavior.

For an easier comparison between a single parameter such as θ_{RO} and the impact behavior which is represented by a large number of experiments in different conditions, one needs to collapse the impact data into a (small set of) meaningful number(s). To this aim, principal component analysis (PCA) was used on the impact data (R_C, N_d, D_{eq}, $V_{R,max}$, ξ_{max}). Principal vectors, forming an orthogonal basis of this five-dimensional parameter space, were selected by maximizing the variance of the data set along them, decreasing from the first (most significant) to the last (least significant) principal component. This analysis was only performed for the wax-based coating type which showed superior performance, and were restricted to $5 < We < 30$, the range in which rebound essentially occurs.

The first principal component (PC1) is $c_1 = 59.8\, R_C + 45.5\, N_d - 55.7\, D_{eq}$; since a higher restitution coefficient R_C, a higher number N_d of droplets (due to splashing or ejection) and a lower equilibrium contact width D_{eq} (*i.e.*, higher static contact angle) indicate a better water-repellency, this first principal component characterizes the goodness of the fabric sample as globally seen in impact experiments. The second principal component (PC2) is $c_2 = 66.3\ V_{R,max} + 64.2\ \xi_{max}$, combining the maximum receding rate $V_{R,max}$ with the dimensionless maximal contact width ξ_{max}. As shown before (Figs. 3 and 5), both parameters are essentially dependent on *We*, with only a slight dependence on fabric roughness for $V_{R,max}$; therefore, c_2 essentially captures the conditions of the impacting droplet which directly govern the spreading and retraction behavior. Together, these two components capture 76.5% of the variance of the data set. As a result, focusing only on them reduces the dimensionality of the parameter space to be visualized without significant loss of information.

Fig. 8a presents the data points plotted in the (c_1,c_2) plane, color-coded by the value of roll-off angle measured on the same fabrics. The data is spread along PC1 according to the value of the roll-off angle, indicating that the θ_{RO} of a fabric may be able to provide an approximate description of how the fabric will interact with droplets in an impact test. This is confirmed when plotting the roll-off angle of fabrics versus the coordinates along the first principal component of a set of rebound experiments performed on the same fabric, showing that lower roll-off angles indeed coincide with higher values along PC1 (Fig. 8b). Hence, the fabrics with lower θ_{RO} are also the ones with a better water repellency behavior as judged from drop impact studies. This points to the fact that the underlying mechanisms which prevent the droplet from rolling off easily also play a role in preventing the droplet from rebounding.

One may thus wonder whether performing a set of rebound experiments provides a real added value compared to a much simpler and faster roll-off experiment. Indeed, since droplets rebound to an approximately constant height independent of *We* (Fig. S4), the only supplementary information contained in a set of rebound experiments is the *We* range over which rebound happens for a given fabric (Fig. 6), and the value of *a* in the scaling relationship $R_C = a\ We^{-1/2}$ which slightly depends on the coating type. This information is thus contained in two

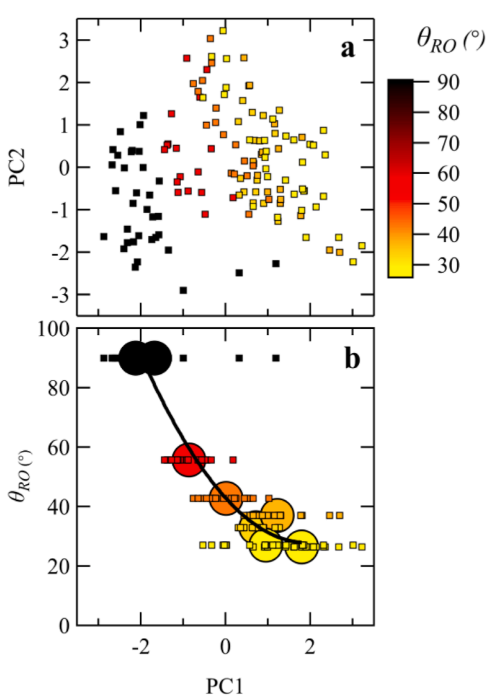

Fig. 8. a. Visual representation of droplet dynamic behavior in different *PhobRSH*-coated fabrics at low *We* ($We < 30$) based on the first two principal components of *PCA*, with roll-off angle θ_{RO} of fabrics as colormap (a value of 90° indicates no roll-off). **b**. Correlation between the roll-off angle measured on a fabric and the PC1 components of rebound experiments performed on the same fabric; the large circles indicate the average PC1 value for each set of experiments on a given fabric; the continuous line is drawn as guide to the eye.

numbers. Additionally, as a comparison of Figs. 6 and 7 shows, when the prefactor *a* of a specific coating type is higher, the *We* range of rebound is also higher on this coating type. Therefore, the two numbers provided by rebound experiments are at least partially correlated. The information contained in an extensive set of rebound experiments is thus not very different from the one provided by a simple roll-off experiment, which provides one number only. This is fully supported by the correlation found in Fig. 8b between rebound behavior and roll-off angle.

Nevertheless, the correlation between rebound and roll-off angle only holds within a series of fabrics modified by the same coating formulation (*PhobRSH* in Fig. 8). When comparing fabrics coated by different formulations, the correlation between rebound behavior and roll-off is lost. For instance, roll-off angles indicate wax-coated fabrics to be superior to *PDMS*-coated ones, followed by *CF4*-modified systems (Fig. 1); whereas Figs. 6 and 7 show that, with respect to rebound, wax-coated fabrics are superior to *CF4*-coated systems, which display better properties than *PDMS*-based coatings. These differences indicate that rebound experiments are sensitive to physical parameters other than the pinning parameter μ (which dominates roll-off). It is likely that viscoelastic dissipation upon droplet impact is one such parameter that controls droplet rebound, adversely affecting *PDMS*-coated fabrics.

4. Conclusions

We have investigated the behavior of droplets impacting fabrics of different roughness and coating type, in a range of impacting conditions for Weber numbers below *ca.* 120 and droplets of size below the capillary length of water, and compared it to measurements of static θ and roll-off θ_{RO} angles. Fabrics with low roughness (below *ca.* 1.3) are in the partially-impregnated regime in static conditions; they display lower θ, no roll-off, a slightly slower retraction rate for impacting droplets, a narrower *We* range in which rebound occurs, and a limited maximum rebound at intermediate *We*. In contrast, rougher fabrics are in a superficially wet state in static conditions; with roughness increasing, they exhibit slightly higher θ, lower roll-off angle, a slightly faster retraction rate for impacting droplets, and a larger *We* range for rebound; additionally, the restitution upon rebound is governed by a $R_C = a\ We^{-1/2}$ scaling law, indicating a near-to-constant rebound height.

In the context of imparting water repellency to fabrics, a higher roughness is thus generally favorable to improve water repellency, because it contributes to entrap air pockets at the fabric surface, which decreases interfacial friction. However, these general conclusions are modulated by details of the fabric texture; in particular, the accumulation of features such as loose threads or dangling fiber ends on the fabric surface, although contributing to increasing the roughness, also results in increased droplet pinning and a deviation from these general conclusions.

As regards coating type, which is of utmost importance for the development of more sustainable water-repellent textiles, we found that roll-off angle, *We* range for rebound, and prefactor *a* of the restitution scaling law are modulated by the coating type, with the wax-based coating being superior to the silicone and perfluorobutyl-based ones in both drop impact and roll-off experiments, although the three coatings are equivalent with respect to the static contact angle. The superiority of wax-based coatings might be related to their lower pinning parameter, which probably results from the crystallization of the wax component which rigidifies the coating and is therefore expected to decrease viscoelastic dissipation upon impact or rolling, compared to the rubbery silicone and short perfluoroalkyl coatings which do not crystallize.

Finally, one should be aware of the limits of the present study, which did not investigate the impact of droplets larger than the capillary length of water, such as found in a heavy rain. Such conditions are likely to result in significantly different scaling laws and results, and remain to be explored further.

Supporting information

TEM image of a cross-section of a dip-coated fabric, profilometry images of fabrics, splashing frequency, maximal rebound height. All recorded videos and extracted parameters are available at https://dataverse.uclouvain.be/dataverse/DropletVideos.

Author contributions

Use this form to specify the contribution of each author of your manuscript. A distinction is made between five types of contributions: Conceived and designed the analysis; Collected the data; Contributed data or analysis tools; Performed the analysis; Wrote the paper.

For each author of your manuscript, please indicate the types of contributions the author has made. An author may have made more than one type of contribution. Optionally, for each contribution type, you may specify the contribution of an author in more detail by providing a one-sentence statement in which the contribution is summarized. In the case of an author who contributed to performing the analysis, the author's contribution for instance could be specified in more detail as 'Performed the computer simulations', 'Performed the statistical analysis', or 'Performed the text mining analysis'.

If an author has made a contribution that is not covered by the five pre-defined contribution types, then please choose 'Other contribution' and provide a one-sentence statement summarizing the author's contribution.

Author 1: Patrick James Cruz

Conceived and designed the analysis

Specify contribution in more detail (optional; no more than one sentence)

Collected the data

Specify contribution in more detail (optional; no more than one sentence)

Contributed data or analysis tools

Specify contribution in more detail (optional; no more than one sentence)

Performed the analysis

Specify contribution in more detail (optional; no more than one sentence)

Wrote the paper

Specify contribution in more detail (optional; no more than one sentence)

Author 2: Pierre-Paul De Breuck

Conceived and designed the analysis

Specify contribution in more detail (optional; no more than one sentence)

Contributed data or analysis tools

Specify contribution in more detail (optional; no more than one sentence)

Performed the analysis

Specify contribution in more detail (optional; no more than one sentence)

Wrote the paper

Specify contribution in more detail (optional; no more than one sentence)

Author 3: Gian-Marco Rignanese

Conceived and designed the analysis

Specify contribution in more detail (optional; no more than one sentence)

Contributed data or analysis tools

Specify contribution in more detail (optional; no more than one sentence)

Performed the analysis

Specify contribution in more detail (optional; no more than one sentence)

Wrote the paper

Specify contribution in more detail (optional; no more than one sentence)

Author 4: Karine Glinel

Conceived and designed the analysis

Specify contribution in more detail (optional; no more than one sentence)

Performed the analysis

Specify contribution in more detail (optional; no more than one sentence)

Wrote the paper

Specify contribution in more detail (optional; no more than one sentence)

Author 5: Alain M. Jonas

Conceived and designed the analysis

Specify contribution in more detail (optional; no more than one sentence)

Contributed data or analysis tools

Specify contribution in more detail (optional; no more than one sentence)

Performed the analysis

Specify contribution in more detail (optional; no more than one sentence)

Wrote the paper

Specify contribution in more detail (optional; no more than one sentence)

Declaration of Competing Interest

The authors declare that they have no known competing financial interests or personal relationships that could have appeared to influence the work reported in this paper.

Data availability

All recorded videos and extracted parameters are available at https://dataverse.uclouvain.be/dataverse/DropletVideos

Acknowledgments

The authors thank Jean-Noël Avril (Decathlon), David De Smet (Centexbel) and Myriam Vanneste (Centexbel) for discussions and the gift of fabrics and coating formulations, and Naïma Sallem, Cécile D'Haese and Delphine Magnin (UCLouvain) for help with contact angle measurements, coating processes and microscopy, respectively. This work was partially financed by the Interreg V program France-Wallonia-Flanders (http://www.interreg-fwvl.eu/nl), a crossborder collaboration program with financial support of the European Fund for Regional Development, and co-financed by the province West Flanders and the Walloon Region through the project Duratex. G.-M. R. is a Research Director of the F. R. S.–FNRS, K. G. is a Senior Research Associate of the F. R. S.–FNRS, and P.-P. DB is Research Fellow of the F.R.S.-FNRS.

Supplementary materials

Supplementary material associated with this article can be found, in the online version, at doi:10.1016/j.surfin.2022.102524.

References

[1] S. Pavlidou, R. Paul, Soil repellency and stain resistance through hydrophobic and oleophobic treatments, in: J.T. Williams (Ed.), Waterproof and Water Repellent Textiles and Clothing, Woodhead Publishing, Duxford, 2018, pp. 73–88, https://doi.org/10.1016/b978-0-08-101212-3.00003-4.

[2] X. Lim, Tainted water: the scientists tracing thousands of fluorinated chemicals in our environment, Nature 566 (2019) 26–29, https://doi.org/10.1038/d41586-019-00441-1.

[3] Commission Regulation (EU) 2017|1000, Official J. Eur. Union. L150 (2017) 14–18. https://data.europa.eu/eli/reg/2017/1000/oj.

[4] S. Brendel, É. Fetter, C. Staude, L. Vierke, A. Biegel-Engler, Short-chain perfluoroalkyl acids: environmental concerns and a regulatory strategy under REACH, Environ. Sci. Eur. 30 (2018) 1–11, https://doi.org/10.1186/s12302-018-0134-4.

[5] European Chemicals Agency, Annex XV Restriction report - Proposal for a restriction - Octamethylcyclotetrasiloxane (D4), decamethylcyclopentasiloxane (D5), dodecamethylcyclohexasiloxane (D6), (2019). https://echa.europa.eu/documents/10162/9a53a4d9-a641-4b7b-ad58-8fec6cf26229.

[6] J. Cai, V. Murugadoss, J. Jiang, X. Gao, Z. Lin, M. Huang, J. Guo, S.A. Alsareii, H. Algadi, M. Kathiresan, Waterborne polyurethane and its nanocomposites: a mini-review for anti-corrosion coating, flame retardancy, and biomedical applications, Adv. Compos. Hybrid Mater. (2022), https://doi.org/10.1007/s42114-022-00473-8 in press.

[7] A.M. Jonas, R. Cai, R. Vermeyen, B. Nysten, M. Vanneste, D.D. Smet, K. Glinel, How roughness controls the water repellency of woven fabrics, Mater. Des. 187 (2020), 108389, https://doi.org/10.1016/j.matdes.2019.108389.

[8] A. Tuteja, W. Choi, G.H. McKinley, R.E. Cohen, M.F. Rubner, Design parameters for superhydrophobicity and superoleophobicity, MRS Bull. 33 (2008) 752–758, https://doi.org/10.1557/mrs2008.161.

[9] Q. Truong, N. Pomerantz, P. Yip, M. Sieber, J.M. Mabry, S.M. Ramirez, Pilot-scale coating of fabrics with fluorodecyl polyhedral oligomeric silsesquioxane/fluoroelastomer blends, Surf. Innov. 2 (2014) 79–93, https://doi.org/10.1680/si.13.00049.

[10] S. Pan, R. Guo, M. Björnmalm, J.J. Richardson, L. Li, C. Peng, N. Bertleff-Zieschang, W. Xu, J. Jiang, F. Caruso, Coatings super-repellent to ultralow surface tension liquids, Nature 17 (2018) 1040–1047, https://doi.org/10.1038/s41563-018-0178-2.

[11] Q.T. Truong, N. Pomerantz, Waterproof and water repellent textiles and clothing, in: J.T. Williams (Ed.), Waterproof and Water Repellent Textiles and Clothing, Woodhead Publishing, Duxford, 2018, pp. 473–531, https://doi.org/10.1016/b978-0-08-101212-3.00016-2.

[12] M.H. Shim, J. Kim, C.H. Park, The effects of surface energy and roughness on the hydrophobicity of woven fabrics, Text. Res. J. 84 (2014) 1268–1278, https://doi.org/10.1177/0040517513495945.

[13] D. Richard, D. Quéré, Bouncing water droplets, Eur. Phys. Lett. 50 (2000) 769–775, https://doi.org/10.1209/epl/i2000-00547-6.

[14] G. Zhang, M.A. Quetzeri-Santiago, C.A. Stone, L. Botto, J.R. Castrejon-Pita, Droplet impact dynamics on textiles, Soft Matter 14 (2018) 8182–8190, https://doi.org/10.1039/c8sm01082j.

[15] Z. Romdhani, A. Baffoun, M. Hamdaoui, S. Roudesli, Drop impact on textile material: effect of fabric properties, Autex Res. J. 14 (2014) 145–151, https://doi.org/10.2478/aut-2014-0010.

[16] C. Stephen, B. Shivamurthy, M. Mohan, A.H.I. Mourad, R. Selvam, B.H. S. Thimmappa, Low velocity impact behavior of fabric reinforced polymer composites– a review, Eng. Sci. 18 (2022) 75–97, https://doi.org/10.30919/es8d670.

[17] A.N. Bako, F. Darboux, F. James, C. Josserand, C. Lucas, Pressure and shear stress caused by raindrop impact at the soil surface: scaling laws depending on the water depth, Earth Surf. Process. 41 (2016) 1199–1210, https://doi.org/10.1002/esp.3894.

[18] W.A. Zisman, Relation of the equilibrium contact angle to liquid and solid constitution, in: F. Fowkes (Ed.), Contact Angle, Wettability, and Adhesion, American Chemical Society, 1964, pp. 1–51, https://doi.org/10.1021/ba-1964-0043.ch001.

[19] R.N. Wenzel, Resistance of solid surfaces to wetting by water, Ind. Eng. Chem. 28 (1936) 988–994, https://doi.org/10.1021/ie50320a024.

[20] A.B.D. Cassie, S. Baxter, Wettability of porous surfaces, Trans. Faraday Soc. 40 (1944) 546, https://doi.org/10.1039/tf9444000546. –6.

[21] E.Y. Bormashenko, Wetting of Real Surfaces, 2nd ed., De Gruyter, 2018.

[22] P.G.D. Gennes, F. Brochard-Wyart, D. Quéré, Capillarity and Wetting Phenomena, Springer, 2004.

[23] C.G.L. Furmidge, Studies at phase interfaces. I. The sliding of liquid drops on solid surfaces and a theory for spray retention, J. Colloid Sci. 17 (1962) 309–324, https://doi.org/10.1016/0095-8522(62)90011-9.

[24] E.B. Dussan, On the ability of drops or bubbles to stick to non-horizontal surfaces of solids. Part 2. Small drops or bubbles having contact angles of arbitrary size, J. Fluid Mech. 151 (2006) 1–20, https://doi.org/10.1017/s0022112085000842.

[25] K.K. Varanasi, T. Deng, M.F. Hsu, N. Bhate, Design of superhydrophobic surfaces for optimum roll-off and droplet impact resistance, in: 2009: pp. 637–645. 10.1115/imece2008-67808.

[26] C. Clanet, C. Béguin, D. Richard, D. Quéré, Maximal deformation of an impacting drop, J. Fluid Mech. 517 (2004) 199–208, https://doi.org/10.1017/s0022112004000904.

[27] T. Bobinski, G. Sobieraj, M. Psarski, G. Celichowski, J. Rokicki, Droplets bouncing on the surface with micro-structure, Arch. Mech. 69 (2017) 177–193.

[28] C. Josserand, S.T. Thoroddsen, Drop impact on a solid surface, Annu. Rev. Fluid Mech. 48 (2015) 1–27, https://doi.org/10.1146/annurev-fluid-122414-034401.

[29] D. Richard, C. Clanet, D. Quéré, Contact time of a bouncing drop, Nature 417 (2002) 811, https://doi.org/10.1038/417811a. –811.

[30] A.-L. Biance, F. Chevy, C. Clanet, G. Lagubeau, D. Quéré, On the elasticity of an inertial liquid shock, J. Fluid Mech. 554 (2006) 47–66, https://doi.org/10.1017/s0022112006009189.

[31] C. Antonini, F. Villa, I. Bernagozzi, A. Amirfazli, M. Marengo, Drop rebound after impact: the role of the receding contact angle, Langmuir 29 (2013) 16045–16050, https://doi.org/10.1021/la4012372.